

# Enhancement mechanism of the electron g-factor in quantum point contacts

Grégoire Vionnet

*School of Physics, The University of New South Wales, Sydney, NSW 2052, Australia and  
Institute of Theoretical Physics, École Polytechnique Fédérale de Lausanne (EPFL), CH-1015 Lausanne, Switzerland*

Oleg P. Sushkov

*School of Physics, The University of New South Wales, Sydney, NSW 2052, Australia*

(Dated: March 6, 2022)

The electron g-factor measured in a quantum point contact by source-drain bias spectroscopy is significantly larger than its value in a two-dimensional electron gas. This enhancement, established experimentally in numerous studies, is an outstanding puzzle. In the present work we explain the mechanism of this enhancement in a theory accounting for the electron-electron interactions. We show that the effect relies crucially on the non-equilibrium nature of the spectroscopy at finite bias.

PACS numbers: 72.25.Dc, 73.23.Ad, 71.70.Gm, 73.21.Hb

A quantum point contact (QPC) is a narrow quasi-1D constriction linking two 2D electron gas (2DEG) reservoirs. It is essentially the simplest mesoscopic system which makes it interesting both for technological applications and on a fundamental level. Experimental studies of QPCs started with the discovery of the quantisation of the conductance in steps of  $G_0 = 2e^2/h$  [1, 2], which is a single-particle effect well understood theoretically [3]. Many-body interactions/correlations in QPCs were first undoubtedly identified in the “0.7-anomaly” of the conductance and the g-factor enhancement [4], and a few years later in the zero bias anomaly (ZBA) of the conductance [5]. Since their discovery, these effects have been the subject of numerous experimental studies, see e.g. Refs. [6–10]. In spite of 20 years of studies there is no consensus about the mechanism of the 0.7 & ZBA. We believe that they are both due to the enhanced inelastic electron-electron scattering on the top of the QPC potential barrier [11–13]. However, there are alternative theoretical models of these effects based on various assumptions, see e.g. Refs. [14–16]. In the present work we do not address the 0.7 & ZBA, but consider the mechanism underlying the electron g-factor enhancement. We show that a simple saddle-point potential model combined with local electronic interactions is sufficient to capture the relevant physics. There are two previous theoretical works related to this problem, Refs. [13, 17]. Ref. [17] considers the usual Landau Fermi liquid exchange interaction mechanism of the g-factor enhancement in an infinitely long quantum wire. This mechanism can hardly be relevant for a QPC since the length of the quasi-1D channel connecting the leads is much shorter than the spin relaxation length. Ref. [13] addresses a real QPC and points out a magnetic splitting enhancement effect. While this effect does exist, we will show below that it is exactly cancelled out in a source-drain bias spectroscopy experiment and therefore does not explain the observed phenomenon.

We consider the conduction band electrons in a semiconductor. Due to the spin-orbit interaction in the valence band, the value of the single electron g-factor can

be very different from its vacuum value. For example in GaAs,  $g_0 = -0.44$  [18]. This value can be measured in fast processes, say in ESR, where  $g_0$  is not renormalised by electron-electron interactions [19, 20]. On the other hand, the static electron g-factor  $g^*$  measured for example via static Pauli magnetisation in an infinite system is enhanced compared to  $g_0$  due to the exchange electron-electron interactions [17, 21]. Considering that the time of flight of an electron through a QPC is of the order of the picosecond, how can the g-factor be renormalised in such a fast process? We show below that the observed enhancement is specific to the source-drain bias spectroscopy method to measure the g-factor in QPCs.

If we neglect the electron-electron interactions in the QPC the problem can be described by the saddle point potential created by the gates

$$V(x, y) = V_0 - \frac{1}{2}m\omega_x^2x^2 + \frac{1}{2}m\omega_y^2y^2, \quad (1)$$

with  $m$  the effective mass of the electron. The electric current flows in the  $x$ -direction from the source to the drain. The potential is separable and the QPC transmission problem is reduced to the solution of a one dimensional Schrödinger equation with effective potential  $U(x)$  [3]. The potential is peaked at  $x = 0$  where

$$U_n(x) \approx U_{0n} - \frac{m\omega_x^2x^2}{2}, \quad U_{0n} = V_0 + \hbar\omega_y(n + 1/2). \quad (2)$$

Here  $n = 0, 1, 2, \dots$  indicates the transverse channel. At an infinitesimally small bias, the conductance is described by the transmission coefficient at the Fermi level. Applying an in-plane magnetic field  $B$  just spin splits the Fermi level  $\epsilon_{\pm} = \mu \pm g^*B/2$  with  $\mu$  the chemical potential and the Bohr magneton set to unity. The splitting is determined by the  $g^*$ -factor which accounts for electron-electron exchange interactions in the leads. The quasi-1D channel has no significant impact on  $g^*$  since its length ( $\sim 100\text{nm}$ ) is much smaller than the spin-relaxation length ( $l_s \sim 10\mu\text{m}$ ). The energies  $\epsilon_{\pm}$  and the potential curves describing the QPC are sketched in Fig.1a.

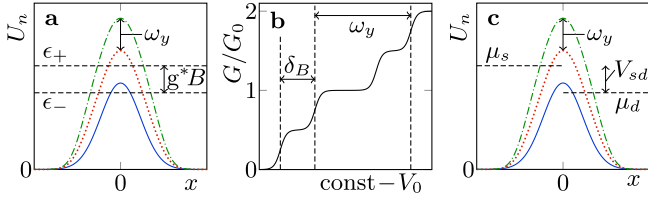


FIG. 1: (a) Potential curves for the transverse channels  $n = 0$  (solid blue),  $n = 1$  (dotted red) and  $n = 2$  (dash-dotted green), and the magnetic field split chemical potential,  $\epsilon_{\pm}$ . (b) Conductance in units of  $G_0 = 2e^2/h$  versus the saddle point potential height  $V_0$ . (c) Similar to (a), but at zero magnetic field and different chemical potentials in the source and drain reservoirs:  $\mu_s - \mu_d = V_{sd}$ .

An electron wave function in a given transverse channel  $n$  is a combination of incident, reflected and transmitted waves. Near the peak of the potential, the wave function with energy  $E_k = k^2/2m$  has the form (for  $k \geq 0$ ) [11]

$$\begin{aligned} \psi_{k,n}(x) &\approx \left(\frac{mv_F^2}{2\omega_x}\right)^{1/4} \varphi_{\epsilon_n}(\xi), \\ \varphi_{\epsilon_n}(\xi) &= \sqrt{\frac{e^{\pi\epsilon_n/2}}{\cosh(\pi\epsilon_n)}} D_\nu(\sqrt{2}\xi e^{-i\pi/4}), \\ \epsilon_n &= (E_k - U_{0n})/\omega_x, \quad \xi = x\sqrt{m\omega_x}. \end{aligned} \quad (3)$$

Here  $v_F$  is the Fermi velocity far from the barrier,  $D_\nu$  is the parabolic cylinder function,  $\nu = i\epsilon_n - \frac{1}{2}$  and  $\hbar = 1$ . The sign of  $k$  indicates whether the electron is incident from the left ( $k \geq 0$ ) or from the right ( $k \leq 0$ ). For our further analysis it is convenient to define the following functions of energy

$$\begin{aligned} \rho(\epsilon_n) &= |\varphi_{\epsilon_n}(0)|^2 \\ \Phi(\epsilon_n) &= \frac{\pi}{2\sqrt{2}} \int_{-\infty}^{\epsilon_n} \rho(\epsilon') d\epsilon' \end{aligned} \quad (4)$$

plotted in Fig.2a. Due to semiclassical slowing, the

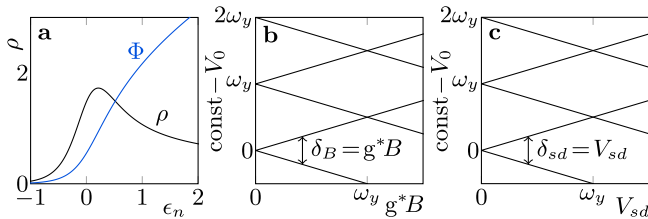


FIG. 2: (a) Probability density at the top of the barrier  $\rho$  and integral of the probability  $\Phi$  versus the electron energy. (b) Position of the conductance steps for non-interacting electrons in the QPC versus  $B$  at infinitesimal  $V_{sd}$ . (c) Similar to (b) but versus the source-drain voltage  $V_{sd}$  at  $B = 0$ .

probability density at the top of the potential barrier,  $|\psi_{k,n}(0)|^2 \propto \rho(\epsilon_n)$ , is peaked at  $\epsilon_n \approx 0.2$  strongly enhancing the interaction effects [11–13]. The function  $\Phi$

is proportional to the total electron density at  $x = 0$  in a given transverse channel.

Before considering the g-factor enhancement, we illustrate the high susceptibility of a QPC to a magnetic field  $B$ . Having the wave functions, it is easy to calculate the induced magnetisation  $M(x, y)$  across the QPC which is directly relevant to the recent NMR experiment in Ref. [22]. Here we consider only the linear response to  $B$ . The only effect of electron-electron interactions is to replace  $g_0 \rightarrow g^*$  (and renormalise  $U_{0n}$  and  $\omega_x$ , see below). The magnetisation in the leads is  $M(\infty, y) = \frac{m}{4\pi} g^* B$  and the magnetisation at the neck of the QPC is  $M(0, 0) = \frac{m}{4\pi} \sqrt{\frac{2\omega_y}{\pi\omega_x}} \rho\left(\frac{\mu - U_{00}}{\omega_x}\right) g^* B$ , assuming that only the  $n = 0$  channel is open. The latter depends significantly on the energy through  $\rho$  and the maximum enhancement is fairly large,  $M(0, 0)/M(\infty, 0) \approx 2.5$  for  $\omega_y/\omega_x \approx 3$ . This single-particle effect is, however, unrelated to the g-factor measurement which we discuss in the next paragraph.

The potential curves in Fig.1a can be lowered and raised by varying the QPC potential height  $V_0$ . When the top of a potential curve crosses either one of the  $\epsilon_{\pm}$  horizontal lines, the conductance is changed by  $G_0/2$ . Each transverse channel leads to two split-steps separated by  $\delta_B$  in  $V_0$ , as illustrated in the plot of the conductance versus  $V_0$  in Fig.1b. Without accounting for the electron-electron interactions in the QPC, the splitting is  $\delta_B = g^* B$ . The standard way to represent Fig.1b is to plot the position of the steps versus magnetic field as shown in Fig.2b. The slope of the lines in Fig.2b is related to the g-factor and this is the basis for the g-factor measurement. Of course, only the absolute value can be determined,  $g \rightarrow |g|$ . Unfortunately, in experiments  $V_0$  is unknown and only the gate voltage  $V_g$  is directly accessible.  $V_0$  is proportional to the gate voltage,  $V_0 = \alpha V_g$ , and a non-equilibrium method known as source-drain bias spectroscopy is used to exclude the unknown coefficient  $\alpha$ . The magnetic field is set to be zero, but a finite bias  $V_{sd}$  directly controlled experimentally is applied across the QPC. The difference between the source and the drain chemical potentials is  $\mu_s - \mu_d = V_{sd}$ , as illustrated in Fig.1c. Similarly to the magnetic splitting case, when the top of a potential curve crosses the  $\mu_s$  or  $\mu_d$  level, the differential conductance is changed by  $G_0/2$ . Again, each transverse channel leads to two split-steps separated by  $\delta_{sd}$  in  $V_0$ . For non-interacting electrons  $\delta_{sd} = V_{sd}$ . The position of the steps versus source-drain voltage is shown in Fig.2c. The QPC g-factor is

$$g_Q = \frac{(d\delta_B/dB)}{(d\delta_{sd}/dV_{sd})} = \frac{(\partial V_g/\partial B)}{(\partial V_g/\partial V_{sd})}, \quad (5)$$

where the derivatives are taken at the same gate voltage. The unknown coefficient  $\alpha$  is cancelled out in the ratio in Eq. (5). Disregarding electron-electron interactions in the QPC,  $g_Q = g^*$ .

Due to the many-body screening, the effective electron-electron Coulomb interaction is short-ranged and can be

approximated by a  $\delta$ -function

$$V^c(x_1, x_2) = \pi^2 \lambda \sqrt{\frac{\omega_x}{m}} \delta(x_1 - x_2). \quad (6)$$

Here we assume that the interaction is diagonal in transverse channels,  $\propto \delta_{n_1, n_2}$ . In principle there is also an off-diagonal interaction, but it does not influence our conclusions and is only relevant when several transverse channels are populated. The dimensionless coupling  $\lambda$  is the four-leg vertex function which generally depends on  $x$  and on the electron energy,  $\lambda \rightarrow \lambda(x, \epsilon)$ . For our purposes we need only  $\lambda(x = 0, \epsilon) = \lambda(\epsilon)$ . We have performed a random phase approximation (RPA) calculation of  $\lambda(\epsilon)$  for the  $n = 0$  channel in GaAs with  $\omega_y/\omega_x = 3$  and  $\omega_x = 1\text{meV}$ , see Appendix B. It turns out that in the present case the results are well approximated by discarding the energy-dependence and taking  $\lambda = 0.25$ . This value agrees with the estimate  $\lambda \sim 0.3/\sqrt{\omega_x}$  (with  $\omega_x$  in meV) in Ref. [11]. We comment further on the  $\epsilon$ -dependence of  $\lambda$  below.

The interaction leads to self-energy corrections to the electron energy,  $\epsilon_k \rightarrow \epsilon_k + \Sigma$ . We first consider the Hartree approximation, for which the self-energy  $\Sigma$  is given by the diagram shown in Fig.3a. This is equivalent to a self-consistent potential of electrons which gives corrections to the height of the potential  $U_{0n}$  and to  $\omega_x$ . We focus on the former. The potential at the top of the barrier is the sum of the potential  $V_0$  created by the gates and the self-consistent potential created by the local density of electrons. In a magnetic field, the conductance steps arise when the top of a potential barrier in Fig.1a touches a horizontal dashed line ( $'\epsilon_+'$  or  $'\epsilon_-'$ ). Hence the conditions for the conductance steps are

$$\begin{aligned} '\epsilon_+' : c_n - \frac{V_0}{\omega_x} &= -\frac{g^*B}{2\omega_x} + 2\lambda \left[ \Phi(0) + \Phi\left(-\frac{g^*B}{\omega_x}\right) \right] \\ '\epsilon_-': c_n - \frac{V_0}{\omega_x} &= \frac{g^*B}{2\omega_x} + 2\lambda \left[ \Phi(0) + \Phi\left(\frac{g^*B}{\omega_x}\right) \right] \end{aligned} \quad (7)$$

where  $c_n$  is a constant that depends on the transverse channel. The  $\Phi(0)$ -terms are due to interactions between electrons with same spins, whereas the  $\Phi(\pm g^*B/\omega_x)$ -terms are due to interactions between electrons with opposite spins. The latter terms yield an additional  $B$ -dependence compared to the non-interacting case. The position of the steps versus magnetic field which follow from Eqs.(7) for  $\lambda = 0.25$  and  $\omega_y/\omega_x = 3$  are shown in Fig.3b by black solid lines. For comparison, the dashed blue lines show the non-interacting case, identical to Fig.2b. Fig.3b indicates a very significant Hartree enhancement of the splitting:  $\delta_B > g^*B$ . In Ref. [13] this effect was reported as enhancement of the  $g$ -factor. However, let us look at how the source-drain normalisation in Eq. (5) influences the answer. The conditions for the source-drain conductance steps in the Hartree approxi-

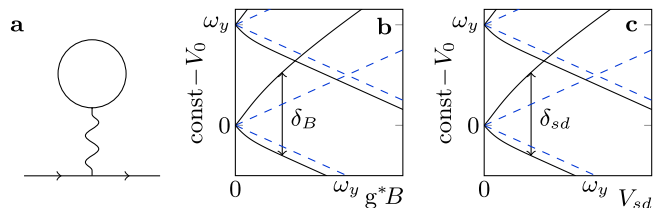


FIG. 3: (a) Hartree self-energy diagram. (b) Position of the conductance steps versus  $B$  at infinitesimal  $V_{sd}$  with the electron-electron interactions in the QPC accounted in the Hartree approximation. Black solid lines correspond to  $\lambda = 0.25$  and  $\omega_y/\omega_x = 3$ . Blue dashed lines correspond to the noninteracting case,  $\lambda = 0$ . (c) Similar to (b) but versus the source-drain voltage  $V_{sd}$  at  $B = 0$ .

mation are

$$\begin{aligned} '\mu_s': c_n - \frac{V_0}{\omega_x} &= -\frac{V_{sd}}{2\omega_x} + 2\lambda \left[ \Phi(0) + \Phi\left(-\frac{V_{sd}}{\omega_x}\right) \right] \\ '\mu_d': c_n - \frac{V_0}{\omega_x} &= \frac{V_{sd}}{2\omega_x} + 2\lambda \left[ \Phi(0) + \Phi\left(\frac{V_{sd}}{\omega_x}\right) \right]. \end{aligned} \quad (8)$$

The factor 2 in front of  $\lambda$  in Eqs.(7) and (8) arises for different reasons. While in Eq.(7) it is due to the left-runners and the right-runners contributing to the density, in Eq. (8) it is due to the two spin polarisations. Due to the coincidence of the prefactors, Eqs. (7) and (8) are identical upon the substitution  $g^*B \leftrightarrow V_{sd}$ . Hence, the plots of the position of the source-drain steps shown in Fig.3c in black solid lines are identical to those in Fig.3b. (Again we show in blue dashed lines the non-interacting case). Therefore in Eq. (5) the ‘‘enhancement’’ is cancelled out and  $g_Q = g^*$ . There is no enhancement of the  $g$ -factor measured by source-drain bias spectroscopy due to the Hartree term. Besides this analytical calculation, we have performed an equilibrium self-consistent Hartree numerical calculation for a realistic QPC in a 3D geometry in the adiabatic approximation, see Appendix A. This numerical calculation supports the above conclusion.

We now account for the Fock exchange term, for which the self-energy diagram is plotted in Fig.4a, and discard the Hartree self-energy. Although in general this contribution to the self-energy leads to a nonlocal potential, in the  $\delta$ -function approximation (6) it becomes a local potential (generally spin-dependent). We can therefore apply the same procedure as in the Hartree case. However, the Fock self-energy is negative and for an electron with a given spin depends only on the density of electrons with the same spin. Therefore, the conditions for the conductance steps in a magnetic field read

$$\begin{aligned} '\epsilon_+' : c_n - \frac{V_0}{\omega_x} &= -\frac{g^*B}{2\omega_x} - 2\lambda\Phi(0) \\ '\epsilon_-': c_n - \frac{V_0}{\omega_x} &= \frac{g^*B}{2\omega_x} - 2\lambda\Phi(0). \end{aligned} \quad (9)$$

It is very similar to the direct interaction case (7), but the sign of the  $\lambda$ -terms is opposite and there is no

term related to interactions between electrons with opposite spins. Therefore the exchange contribution is  $B$ -independent and the position of the conductance steps, shown in Fig.4b, are identical to the non-interacting case, Fig.2b. There is no exchange enhancement of the splitting,  $\delta_B = g^*B$ . This is counterintuitive and very differ-

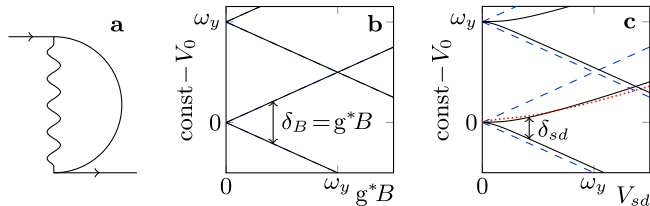


FIG. 4: (a) Fock self-energy diagram. (b) Position of the conductance steps versus  $B$  at infinitesimal  $V_{sd}$  with the electron-electron interactions in the QPC accounted in the Fock approximation. Black solid lines correspond to  $\lambda = 0.25$  and  $\omega_y/\omega_x = 3$ . Blue dashed lines correspond to the noninteracting case,  $\lambda = 0$ . (c) Similar to (b) but versus the source-drain voltage  $V_{sd}$  at  $B = 0$ . The red dotted line accounts for the energy dependence of  $\lambda(\epsilon)$  in the RPA.

ent from what we know well about uniform systems [21]. However, this does not imply that the  $g$ -factor measured by source-drain bias spectroscopy is not changed. At zero magnetic field and finite bias, including the exchange contribution, the conditions for the conductance steps are

$$\begin{aligned} \mu_s' : c_n - \frac{V_0}{\omega_x} &= -\frac{V_{sd}}{2\omega_x} - \lambda \left[ \Phi(0) + \Phi\left(-\frac{V_{sd}}{\omega_x}\right) \right] \\ \mu_d' : c_n - \frac{V_0}{\omega_x} &= \frac{V_{sd}}{2\omega_x} - \lambda \left[ \Phi(0) + \Phi\left(\frac{V_{sd}}{\omega_x}\right) \right]. \end{aligned} \quad (10)$$

Compared to the Hartree case (8), the interaction contributions have opposite signs and there is no factor 2 since only electrons with same spin contribute. The position of the steps versus  $V_{sd}$  is shown in Fig.4c in black solid lines. For comparison, the red dotted line shows a curve taking into account the energy dependence of  $\lambda(\epsilon)$  obtained from the RPA calculation. It is practically indistinguishable from the black solid line, thus justify-

ing approximating  $\lambda$  by a constant. The exchange interaction reduces the splitting  $\delta_{sd}$  compared to the non-interacting case,  $\delta_{sd} < V_{sd}$ . Hence from Eq. (5), the  $g$ -factor is enhanced. With parameters corresponding to the presented plots ( $\lambda = 0.25$ ,  $\omega_y/\omega_x = 3$ ) the  $g$ -factor enhancement is  $g_Q/g^* \approx 1.5 - 2$  in agreement with experiments. By increasing  $\lambda$  one increases the enhancement, but then of course the single loop analysis becomes questionable. When several transverse channels are populated, the screening must reduce the value of  $\lambda$ , thus reducing the  $g$ -factor enhancement in agreement with experiments [4].

We stress that  $g_Q$  is a multiplicative of  $g^*$  which is itself somewhat enhanced compared to  $g_0$  due to the exchange interaction in the leads. Implicit support for our analysis comes from the experiments [23, 24]. They measure the electron  $g$ -factor  $g$  via magnetic field and temperature dependence of the magnetic field induced spin polarisation in QPC injection. This method does not rely on source-drain bias spectroscopy and gives  $g \approx g_0$ . The fact that  $g \neq g_Q$  supports our analysis which is consistent with  $g = g^* \approx g_0$ , see also [25]. An explicit confirmation of our theory would come from a conductance measurement of the  $g$ -factor which does not rely on the source-drain bias spectroscopy.

In conclusion, the  $g$ -factor enhancement in the Hartree-Fock approximation is  $g_Q/g^* = \frac{1+H}{1+H-F} \approx (1+F)$ , where  $H$  and  $F$  are the Hartree and Fock electron-electron interaction contributions respectively. The numerator is due to the magnetic splitting and the denominator is due to the source-drain normalisation. Contrary to naive expectations, the exchange Fock diagrams do not increase the magnetic splitting. However, the exchange diagrams reduce the source-drain splitting in the non-equilibrium procedure used as normalisation of the energy scale, thus explaining the measured  $g$ -factor enhancement. The theoretical value of the enhancement is consistent with experiments.

We are grateful to A. P. Micolich, A. R. Hamilton, S. E. Barnes, A. I. Milstein, and D. A. Ritchie for very important comments and discussions.

- 
- [1] B. J. van Wees, H. van Houten, C. W. J. Beenakker, J. G. Williamson, L. P. Kouwenhoven, D. van der Marel, and C. T. Foxon, *Phys. Rev. Lett.* **60**, 848 (1988).  
[2] D. A. Wharam, T. J. Thornton, R. Newbury, M. Pepper, H. Ahmed, J. E. F. Frost, D. G. Hasko, D. C. Peacock, D. A. Ritchie, and G. A. C. Jones, *J. Phys. C* **21**, L209 (1988).  
[3] M. Büttiker, *Phys. Rev. B* **41**, 7906 (1990).  
[4] K. J. Thomas, J. T. Nicholls, M. Y. Simmons, M. Pepper, D. R. Mace, and D. A. Ritchie, *Phys. Rev. Lett.* **77**, 135 (1996).  
[5] S. M. Cronenwett, H. J. Lynch, D. Goldhaber-Gordon, L. P. Kouwenhoven, C. M. Marcus, K. Hirose, N. S. Wingreen, and V. Umansky, *Phys. Rev. Lett.* **88**, 226805 (2002).  
[6] E. J. Koop, A. I. Lerescu, J. Liu, B. J. van Wees, D. Reuter, A. D. Wieck, and C. H. van der Wal, *J. Supercond. Nov. Magn.* **20**, 433 (2007).  
[7] T.-M. Chen, A. C. Graham, M. Pepper, F. Sfigakis, I. Farrer, and D. A. Ritchie, *Phys. Rev. B* **79**, 081301 (2009).  
[8] C. Rössler, S. Baer, E. de Wiljes, P.-L. Ardelit, T. Ihn, K. Ensslin, C. Reichl, and W. Wegscheider, *New J. Phys.* **13**, 113006 (2011).  
[9] A. P. Micolich, *J. Phys.: Condens. Matter* **23**, 443201 (2011).

- [10] A. M. Burke, O. Klochan, I. Farrer, D. A. Ritchie, A. R. Hamilton, and A. P. Micolich, *Nano Lett.* **12**, 4495 (2012).
- [11] C. Sloggett, A. I. Milstein, and O. P. Sushkov, *Eur. Phys. J. B* **61**, 427 (2008).
- [12] A. M. Lunde, A. De Martino, A. Schulz, R. Egger, and K. Flensberg, *New J. Phys.* **11**, 023031 (2009).
- [13] F. Bauer, J. Heyder, E. Schubert, D. Borowsky, D. Taubert, B. Bruognolo, D. Schuh, W. Wegscheider, J. von Delft, and S. Ludwig, *Nature* **501**, 73 (2013).
- [14] Chuan-Kui Wang and K.-F. Berggren, *Phys. Rev. B* **57**, 4552 (1998).
- [15] B. Spivak and F. Zhou, *Phys. Rev. B* **61**, 16730 (2000).
- [16] K. A. Matveev, *Phys. Rev. Lett.* **92**, 106801 (2004).
- [17] Chuan-Kui Wang and K.-F. Berggren, *Phys. Rev. B* **54**, R14257(R) (1996).
- [18] O. Madelung, *Semiconductors – Basic Data* (Springer, Berlin, 1996).
- [19] Y. Yafet, *Solide State Phys.* **14**, 1 (1963).
- [20] S. E. Barnes, *Adv. Phys.* **30**, 801 (1981).
- [21] J. Janak, *Phys. Rev.* **178**, 1416 (1969).
- [22] M. Kawamura, K. Ono, P. Stano, K. Kono, and T. Aono, *Phys. Rev. Lett.* **115**, 036601 (2015).
- [23] R. M. Potok, J. A. Folk, C. M. Marcus, and V. Umansky, *Phys. Rev. Lett.* **89**, 266602 (2002).
- [24] E. J. Koop, B. J. van Wees, D. Reuter, A. D. Wieck, and C. H. van der Wal, *Phys. Rev. Lett.* **101**, 056602 (2008).
- [25] Ref. [26] while being generally similar to Refs. [23, 24] gives  $g \approx 1.7g_0$  instead of  $g \approx g_0$ . Possibly, this is because in [26] one 2D reservoir is replaced by a  $1\mu\text{m}$ -wide 1D channel, thus enhancing  $g^*$ .
- [26] S. M. Frolov, A. Venkatesan, W. Yu, J. A. Folk, and W. Wegscheider, *Phys. Rev. Lett.* **102**, 116802 (2009).

### Appendix A: Self-consistent Hartree simulation in a realistic 3D geometry

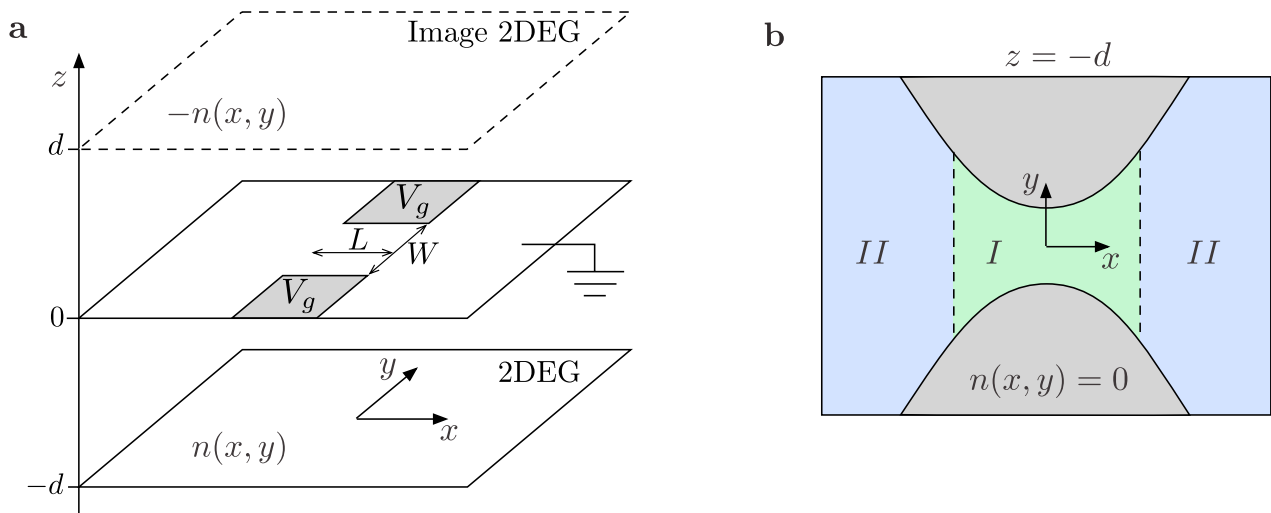


FIG. 5: (a) Model of a QPC as three equidistant two-dimensional layers: a 2DEG, a metallic plate with gates and an image 2DEG. At  $z = 0$ , the gray metal gates have voltage  $V_g$  and the remaining of this plane is grounded. The electron density in the 2DEG at  $z = -d$  is  $n(x, y)$ , whereas in the image 2DEG at  $z = d$  it is  $-n(x, y)$ . (b) Top view of the 2DEG plane ( $z = -d$ ). The gray areas show the completely depleted regions where  $n(x, y) = 0$ . The regions denoted  $I$  (green) and  $II$  (blue) are treated in an adiabatic and Thomas-Fermi approximation respectively.

We consider here a simple electrostatic model of a QPC that takes into account the three-dimensional geometry of the experimental set-up. We focus on the Hartree interaction and ignore any exchange effect. The system is approximated by three equidistant two-dimensional layers, as illustrated in Fig.5a. The 2DEG is situated at  $z = -d$ , and its image is at  $z = d$ . The constriction is formed by applying a potential  $V_g$  on the gray metal gates in the layer at  $z = 0$ . We furthermore impose a zero potential outside of the gates in this plane. The total potential  $U(x, y, z)$  is the sum of the electrostatic potential due to the metal gates and the Hartree potential  $U_H(x, y, z)$  induced by the electrons in the 2DEG and its image. In the plane  $z = 0$ , the total potential reads

$$U|_{z=0} = U_{\text{gates}} = \begin{cases} 0 & \text{outside gates} \\ -eV_g & \text{in gates} \end{cases}. \quad (\text{A1})$$

Writing  $\vec{r}_{\parallel} = (x, y)$ , the induced Hartree potential is

$$U_H(\vec{r}_{\parallel}, z) = \frac{e^2}{4\pi\epsilon_0\epsilon_r} \int d^2\vec{r}'_{\parallel} dz' \frac{n(\vec{r}'_{\parallel})}{\sqrt{|\vec{r}_{\parallel} - \vec{r}'_{\parallel}|^2 + (z - z')^2}} [\delta(z' + d) - \delta(z' - d)]. \quad (\text{A2})$$

This problem is simplest upon Fourier transforming the in-plane coordinates:  $\hat{U}(\vec{q}, z) = \int d^2\vec{r}_{\parallel} U(\vec{r}_{\parallel}, z) e^{i\vec{q}\cdot\vec{r}_{\parallel}}$ . A straightforward calculation yields

$$\hat{U}(\vec{q}) \Big|_{z=-d} = \hat{U}_{\text{gates}}(\vec{q}) e^{-qd} + \frac{e^2}{2\epsilon_0\epsilon_r} \frac{\hat{n}(\vec{q})}{q} (1 - e^{-2qd}) \quad (\text{A3})$$

where  $q = |\vec{q}|$ .

We first describe the simulation at zero bias and then we explain how we treat the non-equilibrium case.

#### 1. Zero bias: $V_{sd} = 0$

We split the in-plane space  $(x, y)$  in regions  $I$  and  $II$  as shown in Fig.5b and use different approximations for the density  $n(x, y)$  in each region. The region  $I$  is defined to be where the approximation  $n_I(x, y)$  used in this region is valid. In region  $II$ , we use the Thomas-Fermi approximation

$$n_{II}(x, y) = \frac{m}{2\pi} \sum_{\sigma=\pm 1} \left( \mu + \sigma \frac{g^* B}{2} - U(x, y) \right) \theta \left( \mu + \sigma \frac{g^* B}{2} - U(x, y) \right) \quad (\text{A4})$$

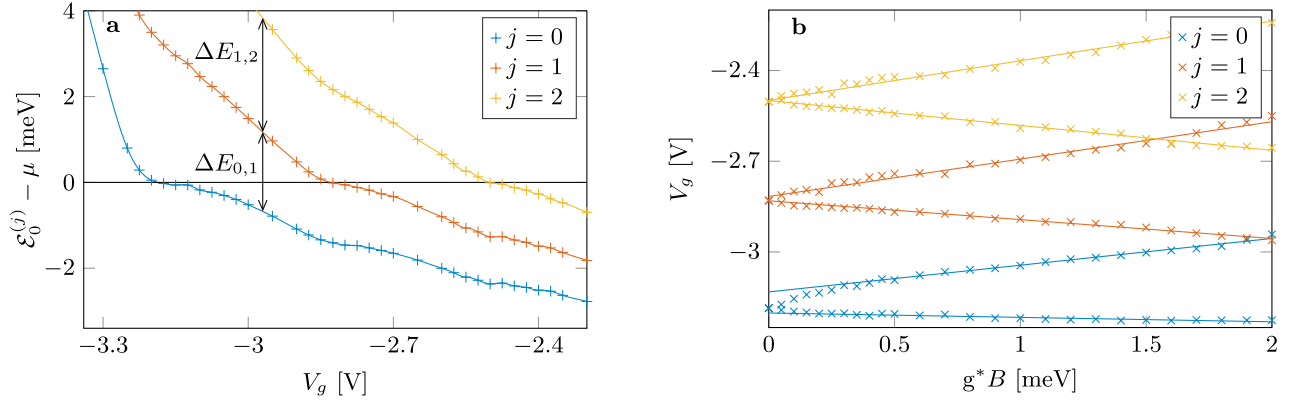


FIG. 6: (a) Potential heights  $\mathcal{E}_0^{(j)}$  of the transverse channels  $j = 0, 1, 2$  as a function of gate voltage  $V_g$ . The solid lines are guides to the eye. (b) Magnetic splitting for the conduction channels  $j = 0, 1, 2$  as a function of the Zeeman splitting  $g^*B$ . The solid lines are linear fits based on the data for  $g^*B > 0.4$  meV.

where  $U(x, y) = U(x, y, -d)$  is the potential in the 2DEG plane. In the region  $I$ , we use the adiabatic approximation and approximate the wavefunctions as  $\Psi_k^{(j)}(x, y) = \psi_k^{(j)}(x)\chi_x^{(j)}(y)$  with  $j$  labelling the transverse channels. The  $\psi_k^{(j)}(x)$  are 1D scattering wavefunctions with the incident part having momentum  $k$  asymptotically far from the constriction. Hence the sign of  $k$  indicates the direction of the incident wave. We first solve numerically the one-dimensional Schrödinger equation at fixed  $x$ :

$$-\frac{1}{2m} \frac{\partial^2 \chi_x(y)}{\partial y^2} + U(x, y)\chi_x(y) = \mathcal{E}_x \chi_x(y). \quad (\text{A5})$$

This yields for each  $x$  a set of eigenfunctions  $\chi_x^{(j)}(y)$  and eigenvalues  $\mathcal{E}_x^{(j)}$  with  $j = 0, 1, 2, \dots$ . The wavefunctions  $\psi_k^{(j)}(x)$  are then found by solving

$$-\frac{1}{2m} \frac{\partial^2 \psi_k^{(j)}(x)}{\partial x^2} + \mathcal{E}_x^{(j)} \psi_k^{(j)}(x) = \frac{k^2}{2m} \psi_k^{(j)}(x) \quad (\text{A6})$$

where the  $x$ -dependent transverse energies  $\mathcal{E}_x^{(j)}$  play the role of an effective potential. Close to the constriction, we can approximate  $\mathcal{E}_x^{(j)} \approx \mathcal{E}_0^{(j)} - \frac{1}{2}m(\omega_x^{(j)})^2 x^2$  for which we know the exact solution as a function of the parabolic cylinder functions. The validity of this harmonic approximation defines the region  $I$ . The density in that region is

$$n_I(x, y) = \sum_{\sigma=\pm 1} \sum_j \sum_{-\infty < k < \infty} |\psi_k^{(j)}(x)|^2 |\chi_x^{(j)}(y)|^2 \theta\left(\mu + \sigma \frac{g^*B}{2} - \frac{k^2}{2m}\right). \quad (\text{A7})$$

The densities  $n_I$  and  $n_{II}$  match pretty smoothly at the boundaries between regions  $I$  and  $II$ .

The self-consistent equation (A3) is solved iteratively with the parameters (see Fig.5a):  $L = 300\text{nm}$ ,  $W = 500\text{nm}$ ,  $d = 90\text{nm}$ ,  $\mu = 6\text{meV}$ ,  $\epsilon_r = 13$  and  $m = 0.07m_e$ . This yields the density  $n_\infty = 1.75 \cdot 10^{11} \text{ cm}^{-2}$  asymptotically far from the constriction. The potential heights  $\mathcal{E}_0^{(j)}$  for the three first transverse channels are shown as a function of gate voltage in Fig.6a. The energy levels are roughly equidistant,  $\Delta E_{0,1}(V_g) \approx \Delta E_{1,2}(V_g)$  (see Fig.6a), and evolve slowly with  $V_g$ , in agreement with experiments. The magnetic splitting in this self-consistent Hartree simulation is shown in Fig.6b. It shows a linear splitting, at least for large enough  $B$ , as observed experimentally. Comparison with the bare electrostatic potential from the gates, i.e. disregarding  $U_H$ , we find a largely enhanced magnetic splitting:  $\delta_B \sim 10 g^*B$ .

## 2. Finite bias: $V_{sd} \neq 0$

We restrict the discussion here to zero magnetic field. In the region  $I$ , we have for  $V_{sd} \neq 0$

$$n_I(x, y) = 2 \sum_j |\chi_x^{(j)}(y)|^2 \left\{ \sum_{k>0} |\psi_k^{(j)}(x)|^2 \theta\left(\mu_s - \frac{k^2}{2m}\right) + \sum_{k<0} |\psi_k^{(j)}(x)|^2 \theta\left(\mu_d - \frac{k^2}{2m}\right) \right\} \quad (\text{A8})$$

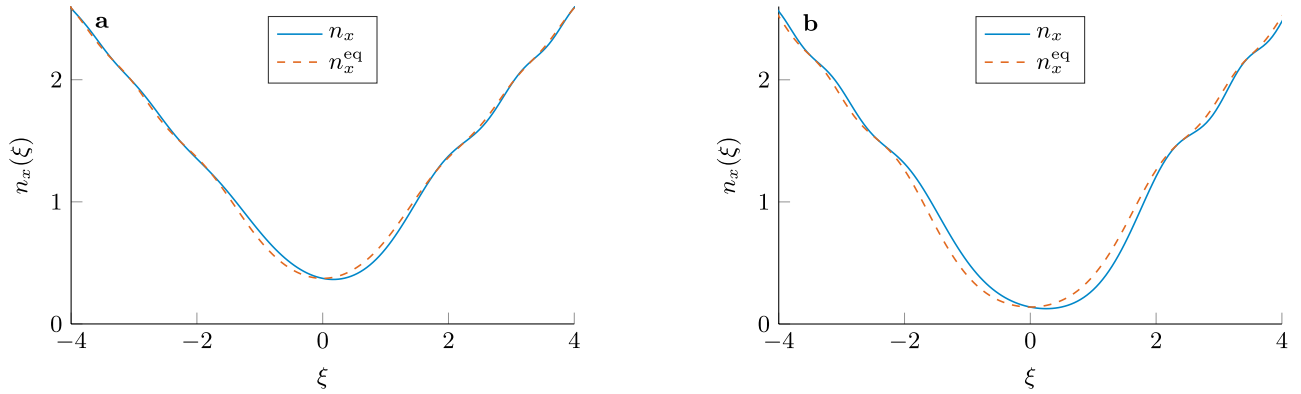


FIG. 7: Comparison between the out-of-equilibrium 1D density  $n_x$  and equilibrium approximation  $n_x^{\text{eq}}$ , using as unit length the dimensionless  $\xi = \sqrt{m\omega_x}x$ . The chemical potentials are: (a)  $\mu_s - \mathcal{E}_0 = 0.4\omega_x$  and  $\mu_d - \mathcal{E}_0 = 0$ ; (b)  $\mu_s - \mathcal{E}_0 = 0$  and  $\mu_d - \mathcal{E}_0 = -0.4\omega_x$ .

where the factor 2 comes from the spin degeneracy. However, we cannot write such an out-of-equilibrium expression for the density in the region  $II$  since the Thomas-Fermi approximation assumes local equilibrium. Therefore our method cannot treat a non-equilibrium situation and we need a simplifying approximation. We are mostly interested in what happens close to the top of the potential, i.e. for small  $|x|$ . We therefore average symmetrically around  $x = 0$ ,

$$n(x, y) \rightarrow \frac{1}{2}(n(x, y) + n(-x, y)) . \quad (\text{A9})$$

To justify this substitution, let's consider the one-dimensional density for a single transverse channel

$$n_x(x) = \sum_{k>0} |\psi_k(x)|^2 \theta(\mu_s - \frac{k^2}{2m}) + \sum_{k<0} |\psi_k(x)|^2 \theta(\mu_d - \frac{k^2}{2m}) \quad (\text{A10})$$

and its equilibrium approximation  $n_x^{\text{eq}}(x) = \frac{1}{2}(n_x(x) + n_x(-x))$ . Considering a parabolic potential barrier, these 1D densities can be expressed in dimensionless densities with  $\xi = \sqrt{m\omega_x}x$ . They are compared in Fig.7 for the cases  $\mu_s - \mathcal{E}_0 = 0.4\omega_x$ ,  $\mu_d - \mathcal{E}_0 = 0$  and  $\mu_s - \mathcal{E}_0 = 0$ ,  $\mu_d - \mathcal{E}_0 = -0.4\omega_x$ . The equilibrium approximation moves some electrons from the source ( $x < 0$ ) to the drain ( $x > 0$ ). Note that the equilibrium approximation is exact at  $x = 0$ .

Since  $\psi_k^{(j)}(-x) = \psi_{-k}^{(j)}(x)$ , the substitution (A9) yields

$$n_I(x, y) \rightarrow \sum_{\sigma=\pm 1} \sum_j \sum_{-\infty < k < \infty} |\psi_k^{(j)}(x)|^2 |\chi_x^{(j)}(y)|^2 \theta(\mu + \sigma \frac{V_{sd}}{2} - \frac{k^2}{2m}) \quad (\text{A11})$$

and similarly

$$n_{II}(x, y) \rightarrow \frac{m}{2\pi} \sum_{\sigma=\pm 1} \left( \mu + \sigma \frac{V_{sd}}{2} - U(x, y) \right) \theta\left( \mu + \sigma \frac{V_{sd}}{2} - U(x, y) \right) . \quad (\text{A12})$$

These formulae are the same as in the case of zero bias and the source-drain splitting can be exactly mapped to a magnetic splitting by  $eV_{sd} \leftrightarrow g^*B$ . Therefore, in the present Hartree approximation,  $g_Q = g^*$  exactly. This is consistent with the perturbative analysis presented in the main text.



## Appendix B: Random Phase Approximation for the electron-electron interaction

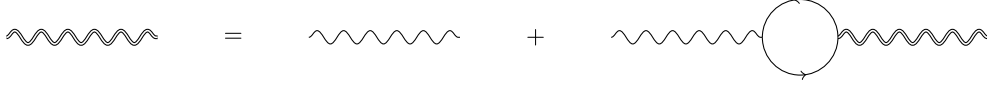


FIG. 8: Diagrammatic representation of the Dyson self-consistent equation for the screened interaction in the RPA.

We detail here a random phase approximation (RPA) calculation of the screened Coulomb interaction for electrons in the lowest transverse channel ( $n = 0$ ) and use it to justify the  $\delta$ -function model presented in the main text.

The 2D wavefunction for the lowest transverse channel is  $\Psi_{k,0}(x, y) = \psi_{k,0}(x)\chi_0(y)$  with  $\chi_0(y) = \left(\frac{m\omega_y}{\pi}\right)^{\frac{1}{4}} e^{-\frac{m\omega_y y^2}{2}}$ . The 1D bare Coulomb interaction is obtained by averaging over the transverse direction:

$$V_0^c(x, x') = \frac{e^2}{4\pi\epsilon_0\epsilon_r} \int dy \int dy' \frac{|\chi_0(y)|^2 |\chi_0(y')|^2}{\sqrt{(x-x')^2 + (y-y')^2}}. \quad (\text{B1})$$

In dimensionless lengths  $\xi = x\sqrt{m\omega_x}$ ,

$$V_0^c(\xi, \xi') = \omega_x \Lambda f\left(\xi - \xi', \frac{\omega_y}{\omega_x}\right) \quad (\text{B2})$$

with  $\Lambda = \frac{e^2}{4\pi\epsilon_0\epsilon_r} \sqrt{\frac{m}{\omega_x}} \approx 3.35$  for typical experimental parameters in GaAs ( $\epsilon_r = 13$ ,  $m = 0.07m_e$ ,  $\omega_x \approx 1\text{meV}$ ) and

$$f(\xi, \alpha) = \frac{\alpha}{\pi} \int d\eta \int d\eta' \frac{e^{-\alpha(\eta^2 + \eta'^2)}}{\sqrt{\xi^2 + (\eta - \eta')^2}} \rightarrow \begin{cases} \frac{1}{|\xi|} & |\xi| \rightarrow \infty \\ \sqrt{\frac{2\alpha}{\pi}} |\ln|\xi|| & |\xi| \rightarrow 0 \end{cases}. \quad (\text{B3})$$

Here  $\alpha = \omega_y/\omega_x$ . Furthermore, because the QPC is not isolated, there will be an additional screening from the metal gates that will be important for large  $|\xi|$ . We model this qualitatively by using the bare interaction

$$V_0^c(\xi, \xi') = \omega_x \Lambda f\left(\xi - \xi', \frac{\omega_y}{\omega_x}\right) e^{-\frac{(\xi - \xi')^2}{\tau^2}} = \omega_x \tilde{V}_0^c(\xi, \xi') \quad (\text{B4})$$

with  $\tau = 10$ . The somewhat arbitrary choice of  $\tau$  has, however, very little influence on the results presented below.

The screened interaction  $V^c(\xi, \xi') = \omega_x \tilde{V}^c(\xi, \xi')$  is found by solving numerically the Dyson self-consistent equation

$$\tilde{V}^c(\xi, \xi') = \tilde{V}_0^c(\xi, \xi') + \int d\xi_1 d\xi_2 \tilde{V}_0^c(\xi, \xi_1) \Pi(\xi_1, \xi_2) \tilde{V}^c(\xi_2, \xi'). \quad (\text{B5})$$

The RPA approximation of this relation is depicted diagrammatically in Fig.8. In this approximation, the static polarisation reads,

$$\Pi(\xi_1, \xi_2) = \sum_{\sigma=\pm 1} \sum_{\delta_1, \delta_2=\pm} \int_{-\infty}^{\tilde{\mu} + \sigma \frac{g^* B}{2\omega_x}} \frac{d\epsilon_1}{2\pi} \int_{\tilde{\mu} + \sigma \frac{g^* B}{2\omega_x}}^{\infty} \frac{d\epsilon_2}{2\pi} \frac{\phi_{\epsilon_2, \delta_2}(\xi_1) \phi_{\epsilon_2, \delta_2}^*(\xi_2) \phi_{\epsilon_1, \delta_1}(\xi_2) \phi_{\epsilon_1, \delta_1}^*(\xi_1)}{\epsilon_1 - \epsilon_2} \quad (\text{B6})$$

where  $\tilde{\mu} = \frac{\mu - U_{00}}{\omega_x}$  and the  $\delta_j = \pm$  indicate the sign of  $k$ , i.e. the direction of the electron.

Because the system is non-uniform, the polarisation is not uniform and  $V^c(\xi, \xi') \neq V^c(\xi - \xi')$ . The dimensionless interaction  $\tilde{V}^c(0, \eta)$  between an electron at the centre of the QPC and an electron at position  $\eta$  is compared to the bare interaction in Fig.9a for  $\tilde{\mu} = 0$ ,  $B = 0$  and  $\omega_y = 3\omega_x = 3\text{meV}$ . The dimensionless interaction  $\tilde{V}^c(1, \eta)$  between an electron at  $\xi = 1$  and an electron at position  $\eta$  for the same parameters is shown in Fig.9b.

The short-ranged screened interaction justifies the  $\delta$ -function approximation

$$V^c(\xi, \xi') \rightarrow \omega_x \pi^2 \lambda(\xi, \tilde{\mu}, B) \delta(\xi - \xi') \quad (\text{B7})$$

with the coupling constant

$$\lambda(\xi, \tilde{\mu}, B) = \frac{1}{\pi^2} \int_{-\infty}^{\infty} \tilde{V}^c(\xi, \eta) d\eta. \quad (\text{B8})$$

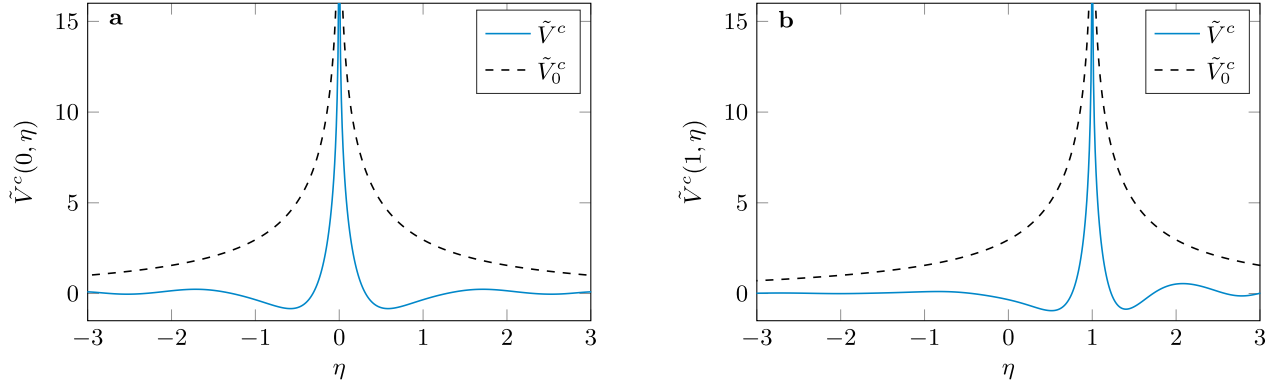


FIG. 9: (a) Screened and bare dimensionless interactions between an electron at the centre of the QPC and an electron at position  $\eta$  for  $\tilde{\mu} = 0$ ,  $B = 0$  and  $\omega_y = 3\omega_x = 3\text{meV}$ . (b) Same as (a) but for an electron at  $\xi = 1$  and an electron at position  $\eta$ .

The coupling constant at  $\xi = 0$  and  $\xi = 1$  is plotted as a function of  $\tilde{\mu}$  in Fig.10a for  $B = 0$ . As  $\tilde{\mu}$  becomes negative and the constriction depopulates, the screening becomes less effective. For  $\tilde{\mu} \lesssim -0.5$ , the contact approximation becomes questionable as the screened interaction gets longer-ranged and eventually tends to the bare interaction. This is qualitatively different from the RPA result for a uniform quantum wire which predicts an unphysical vanishing coupling constant as the density vanishes (as a consequence of the divergence of the density of state). This issue does not arise in the present case of a QPC.

In the magnetic splitting, the step-positions (for the lowest transverse channel) are obtained when  $\epsilon_+ = U_{00}$  (lower line going down in e.g. Fig.3b of the main text) or  $\epsilon_- = U_{00}$  (lower line going up). The coupling constant  $\lambda$  as a function of magnetic field  $B$  with either one of these conditions satisfied is shown in Fig.10b. This result applies also to the source-drain splitting ( $\epsilon_{\pm} \rightarrow \mu_{s/d}$ ,  $g^*B \rightarrow V_{sd}$ ) by applying an analogous equilibrium approximation as in section A 2. Remarkably, even though the coupling  $\lambda$  can in principle vary significantly, as in Fig.10a, it only varies by  $\lesssim 20\%$  in the equations determining the position of the conduction steps in the source-drain bias spectroscopy experiment. Furthermore, the interaction effect is most important for the lines going up and large  $B$  (or  $V_{sd}$ ), thus explaining why there is almost no perceptible difference in Fig.4c of the main text between the result with energy-dependent coupling (red dots) and with constant coupling  $\lambda = 0.25$  (black lines).

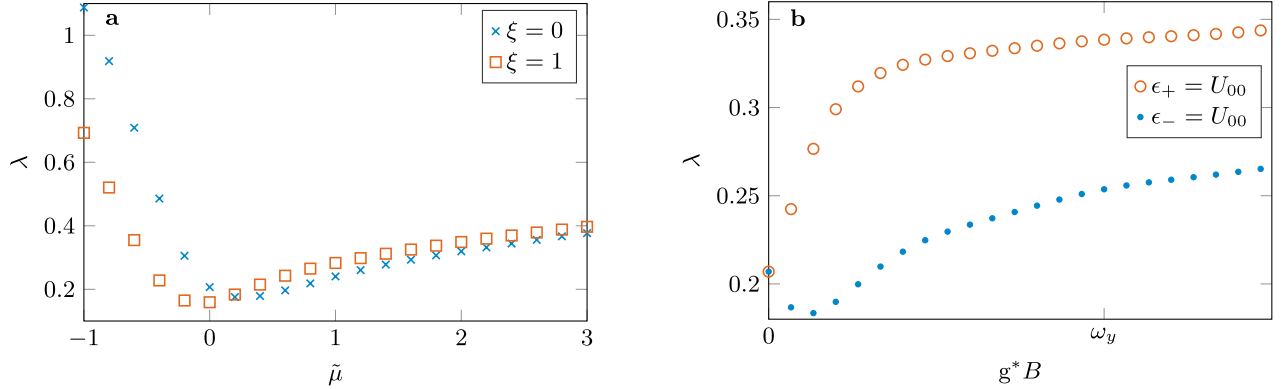


FIG. 10: (a) Coupling constant  $\lambda(\xi, \tilde{\mu}, B)$  at  $\xi = 0$  (centre of the QPC) and  $\xi = 1$  as a function of  $\tilde{\mu}$  for  $\omega_y = 3\omega_x = 3\text{meV}$  and  $B = 0$ . (b) Coupling constant  $\lambda(\xi, \tilde{\mu}, B)$  at the centre of the QPC ( $\xi = 0$ ) as a function of the magnetic field  $B$  at the positions of conductance steps. The condition  $\epsilon_- = U_{00}$  yields the lower line going up (in e.g. Fig.3b of the main text) whereas the condition  $\epsilon_+ = U_{00}$  yields the lower line going down.